A Study on The Use of UAV Images to Improve the Separation Accuracy of Agricultural Land Areas

Fahime Arabi Aliabad
Yazd University
Hamid Reza Ghafarian Malamiri (hrghafarian@yazd.ac.ir)
Yazd University
Saeed Shojaei
Yazd University

Research Article

Keywords: UAV image, Landsat 8, Image fusion methods, Pistachio, Land use

Posted Date: March 11th, 2021

DOI: https://doi.org/10.21203/rs.3.rs-261459/v1

A study on the use of UAV images to improve the separation accuracy of agricultural land areas

Fahime Arabi Aliabad[1], Hamidreza Ghafarian Malamiri[2 *], Saeed Shojaei

1.Department of Arid Lands Management, Faculty of Natural Resources and Desert Studies, Yazd University, Yazd, Iran

2. Department of Geography, Yazd University, Yazd, Iran. (hrghafarian@yazd.ac.ir)

3. Department of Management of Arid and Desert Regions, College of Natural Resources and Desert, Yazd University, Yazd, Iran

Abstract

Classifying satellite images with medium spatial resolution such as Landsat, it is usually difficult to distinguish between plant species, and it is impossible to determine the area covered with weeds. In this study, a Landsat 8 image along with UAV images was used to separate pistachio cultivars and separate weed from trees. In order to use the high spatial resolution of UAV images, image fusion was carried out through high-pass filter, wavelet, principal component transformation, BROVEY, IHS and Gram Schmidt methods, and ERGAS, RMSE and correlation criteria were applied to assess their accuracy. The results represented that the wavelet method with R2, RMSE and ERGAS 0.91, 12.22 cm and 2.05 respectively had the highest accuracy in combining these images. Then, images obtained by this method were chosen with a spatial resolution of 20 cm for classification. Different classification methods including unsupervised method, maximum likelihood, minimum distance, fuzzy artmap, perceptron and tree methods were evaluated. Moreover, six soil classes, Ahmad Aghaei, Akbari, Kalleh Ghoochi, Fandoghi and a mixing class of Kalleh Ghoochi and Fandoghi were applied and also three classes of soil, pistachio tree and weeds were extracted from the trees. The results demonstrated that the fuzzy artmap method had the highest accuracy in separating weeds from trees, differentiating various pistachio cultivars with Landsat image and also classification with combined image and had 0.87, 0.79 and 0.87 kappa coefficients respectively. The comparison between pistachio cultivars through Landsat image and combined image showed that the validation accuracy obtained from harvest has raised by 17% because of combination of images. The results of this study indicated that the combination of UAV and Landsat 8 images affects well to separate pistachio cultivars and determine the area covered with weeds.

Keywords: UAV image; Landsat 8; Image fusion methods; Pistachio; Land use.

Introduction

Accurate data and statistics could be really important to manage agricultural land areas well (Wardlow et al., 2007) Also, the accurate classified information on a variety of agricultural crops plays a significant role in managing agricultural land areas and it can help evaluate net national product. Precision agriculture (PA) can also help experts maximize production efficiency by providing instant information on cultivated land (Hamidy et al., 2016).

The traditional methods applied only through observation of the land to estimate the cultivation area and classification of tree cultivars were very high-priced, time consuming, and not widely applicable. Experts used remote sensing data to discover the type and level of cultivation of each crop, which could give proper information to decision makers (Tatsumi et al., 2015). Satellite data decreases not only human error, but also it can affect in various agricultural programs and lower costs and time.

Since there is a balance in the design of satellites between spatial, temporal, and spectral separation power (Emelyanova et al., 2015), because of technical limitations, most satellites cannot simultaneously bring images together with high spatial, temporal, and spectral resolution, and this is a major limitation in using satellite images.

Nowadays, as science advances, there has been access to aerial images taken by UAVs[1] (Chianucci et al., 2016). One of the biggest advantages of UAV images to satellite images is the determination of the imaging time, high spatial resolution, no restrictions on climatic conditions (cloud cover, etc.) (Zhou et al., 2018). However, taking large-scale UAV images is often expensive and time consuming. One of the most innovative ways is the fusion of UAV and satellite images in order to improve spectral resolution. The fusion of images is a process of mixing two or more images with various spatial and spectral separation in order to provide a new multispectral image by a variety of algorithms (Walker et al., 2014).

[1] Unmanned Aerial Vehicle

The algorithms are divided into three general categories in order to combine images: A) Methods based on substitution such as IHS[2], PCS[3], PCA[4], Gram Schmidt (Shettigara, 1992). B) Multiplication-based methods like Brovey and SVR[5] (Pohl & Van Genderen, 1998). C) Multi-precision decomposition methods, in which spatial features are extracted from a monochrome image and applied to multispectral images (Wilson et al., 1997). During the past three decades, many researchers have suggested different methods for image fusion to raise the spatial resolution of multidimensional images (Barbedo et al., 2019). Yilmaz et al. (2019) studied different methods of combining Worldview as well as UAV images. The results indicated that wavelet and HCS[6] fusion methods were more accurate than other ones. Murugan et al. (2016 and 2017) studied the how to combine UAV and Landsat 8 satellite images and realized that the fusion of these two images could be a great solution in order to monitor the crops accurately and it would be an appropriate way for separation of dense and scattered coatings. Jenerowicz et al. (2017) argued that Gram Schmidt method would be suitable to combine UAV and Landsat 8 images. Agarwal et al. (2018) analyzed the limitations of classification methods for accurate agricultural monitoring using Sentinel 2 satellite and UAV images and believed SVM[7] method would be the most accurate method to classify images obtained by combining UAVs and Sentinels. Zhao et al. (2019) classified the crops precisely by combining UAV and Sentinel 2 images and classified the images of UAVs with spatial resolution of 0.03, 0.10, 0.50, 1.00 and 3.00 m. The results showed that the combined image with spatial resolution of 0.03 demonstrates the most accurate information. In another research, after UAV images were combined with satellite images to create image-based (red, green, and blue) RGB and detect the distance between rows of crops, the results showed that the DSM-based method has far better accuracy compared to the RGB method (Fareed & Rehman, 2020). Since UAV images have not been combined with satellite images to distinguish tree species in weed areas, the aim of this study was to investigate the feasibility of combining UAV images with satellite images

[2] The Intensity-Hue-Saturation
[3] Principal Component *Substitution*
[4] Principal component analysis
[5] Synthetic variable ratio
[6] Hyperspherical color space
[7] Support Vector Machine

to increase the accuracy of classification of different pistachio cultivars and separate weeds from trees. Therefore, a combination of UAV and Landsat 8 images was first used to classify farm density. Then the pistachio cultivars and the weed area were separated at the same time. The results of this study can be used in planning and managing farms and also it can be applied to compare the production of different cultivars.

2. Materials and methods

2.1. Area of study and data sources

The region under study with an area of 423 hectares is situated in the southwest of Yazd province and on the edge of Abarkooh desert. The region is located at longitude 53° 42' 15" to 53° 44' 00" and latitude 31° 14' 15" to 31° 16' 00". The average annual rainfall at the nearest weather station is 65 mm and generally it has a hot and dry climate. The area under study is a pistachio farm that is irrigated by drip irrigation and different pistachio cultivars are cultivated there. Figure 1 shows the location of the area in Iran and Yazd province. Moreover, the supplied UAV and Landsat 8 images have been shown on this figure.

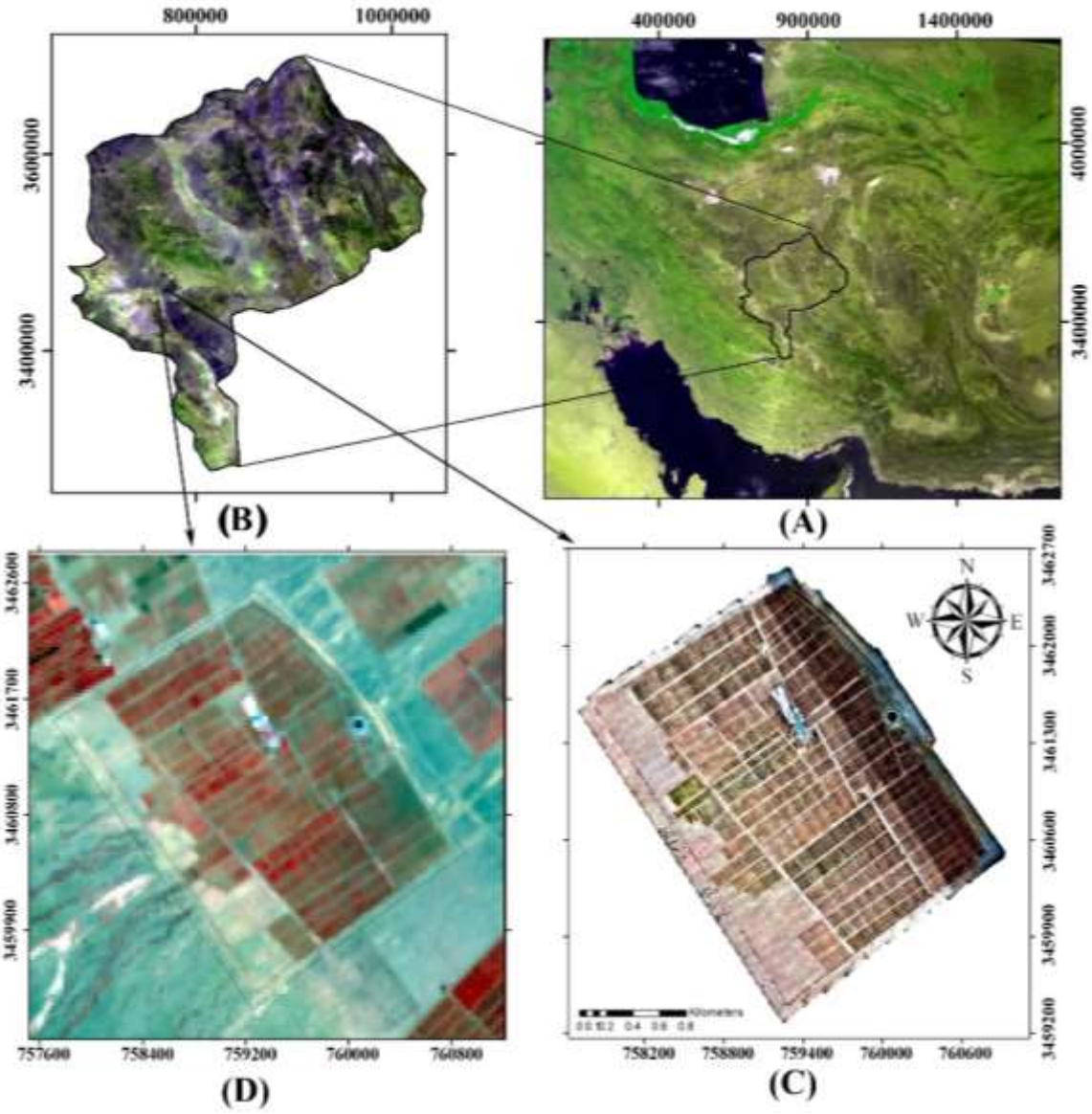

Figure 1. The study area A) Iran B) Yazd province C) Landsat image D) UAV image (08/18/2019)

An OLI[8] image of Landsat 8 satellite and a UAV image were used in order to classify different cultivars of the pistachio tree and also to separate the weeds around the trees. OLI sensors of Landsat 8 gather data for spatial resolution of 30 meters and 8 bands in the visible spectrum, near-infrared, infrared short wavelength and a panchromatic band with a spatial resolution of 15 meters. The UAV image used is an RGB color image, the general specifications of which are given in Table 1. Images of the UAV were taken using Canon

[8] Operational Land Imager

EOS M3 18-55 Digital Camera, the general specifications of which are given in Table 2. The date of imaging was chosen in summer and at the peak of vegetation period. Pistachio phenology includes steps; bloom, leaf out, shell expansion, shell hardening, nut filling, shell splitting, null split, harvest and postharvest. In order to classification, the images related to the nut filling stage have been used, which according to the studies done by Goldhammer, (2005) the peak of vegetation period is related to this stage. Figure 2 shows the diagram of the present study steps.

Table 1. General specifications of the images used

General specification of images applied in the study			
	Spatial resolution	Date	Number of bands
Landsat 8	30 meters	2019-8-18	11
UAV	20 cm		3

Table 2. General specifications of the camera used in the UAV

General specifications of the camera used								
Sensor type	Sensor dimensions	Aperture range	Focal length	Maximum photo resolution	Effective sensor accuracy	Sensor accuracy	Optical zoom	Minimum normal focusing distance
	22.3 × 14.9 mm	F3.5–6.3, F22–40	15 - 45 mm	4000×6000	24.2 MP	24.7 MP	3 times	25 cm

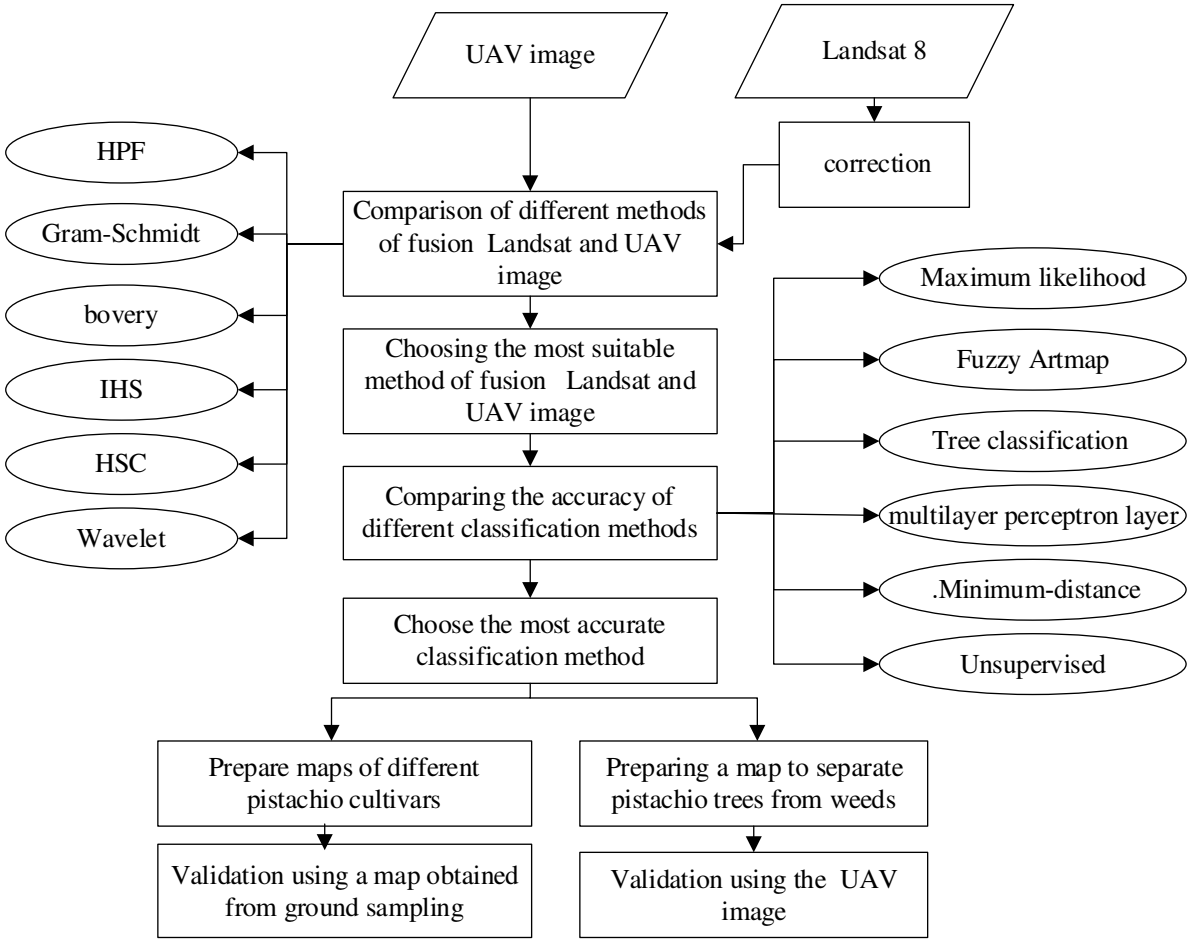

Figure 2. General perspective of the research steps

2.2. Image fusion methods

Image fusion is a useful way to provide a more accurate classification which could be an efficient tool to raise the spatial resolution of multispectral images through two images with different spatial, spectral, and temporal resolution. The history of image fusion goes back to the 1950s and 1960s, and it was started to identify the natural and artificial topography, and also the image fusion of different sensors (Wald, 1999).

2.2.1. Gram-Schmidt method

Gram-Schmidt method has been one of the most popular methods for image fusion since 1998 (Laben & Brower, 2000). The steps for combining multispectral images with a panchromatic image in this method

115 are as follows: 1) simulating a panchromatic image of a spectral band with low spatial resolution 2)
116 Applying GS[9] to a simulated panchromatic image and spectral band using simulation panchromatic band
117 as the first band 3) replacing the high-resolution panchromatic band with the first GS band 4) Using reverse
118 GS to create a panchromatic spectral band (Maurer, 2013). The equation for simulating a panchromatic
119 image using a linear relationship with n multispectral image bands is as follows:

120

121 (1) $$PAN' = \sum_{i=1}^{n} w_i MS_i$$

122

123 Where PAN is the simulated panchromatic image, i = {1, 2,…, n} is the number of multispectral bands, w
124 is the weighted coefficient and MS is the multispectral image band (Aiazzi et al., 2007).

125

126 2.2.2. Fusion of High-Pass Filter (HPF)

127 In this method, a high-pass filter is used to get the details of the spatial information of the image with high
128 spatial resolution and to apply those details to the multispectral image (Pohl & van Genderen, 2014). The
129 image created this way is the same as the original multidimensional image, to which the details of the spatial
130 information of the panchromatic image have been added. This method includes the following steps: 1)
131 Applying the high-pass filter on the panchromatic image with high spatial resolution 2) Adding the filtered
132 image to all multispectral images by applying a weighted coefficient on the standard deviation of
133 multispectral bands 3) Adapting the histogram of the combined image with original multispectral image.
134 The HPF method is based on increasing the spatial resolution of a multispectral image using a high-pass

[9] Gram-Schmidt

filter that extracts high-frequency information and then applies a multispectral image to each band. The general equation for image fusion through method is based on Equation 2.

(2) $$MS_{HPF} = MS_{res} + PAN\_HPFw$$

In which MSHPF is the image obtained by combining with the high-pass filter method, MS_{res} is a multispectral image measured with a panchromatic image, PAN_HPF is a panchromatic image with the application of a high-pass filter, and w is calculated as a weighted coefficient, which is calculated from Equation 3.

(3) $$w_i = \frac{\sigma_{MSi}}{\sigma_{PAN\_HPF}}$$

Where σ_{MSi} is the standard deviation of multispectral image bands and σ_{PAN_HPF} is the standard deviation of the panchromatic image by applying a high-pass filter. In order to implement the HPF method successfully, the size of the main core filter must be specified, which depends on the R factor.

(4) $$R = \frac{PR_{MS}}{PR_{PAN}}$$

Where PR_{MS} is a multispectral image and PR_{PAN} is a panchromatic image and the optimal size of the core is R2 (Aiazzi et al., 2007).

3.2.2. IHS Method

The IHS fusion method is one of the most common methods for combining remote sensing images, and this algorithm has been used widely due to the high spatial resolution of the output image and the high efficiency of this algorithm in satellite images (Carper et al., 1990). In fact, IHS is a spectral replacement method that extracts spatial (I) and spectral information (H, S) from a standard RGB image. This method converts the multispectral image color space from RGB space to IHS space, replaces its spatial component with panchromatic image, and then applies reverse conversion and returns to RGB color space (Zhang et al., 2008). The mathematical principles of this method are based on Equations 5, in which I represent the intensity, H the color, S the saturation, and v1 and v2 represent the intermediate variables required to convert (Pohl & Van Genderen, 1998).

$$\begin{bmatrix} I \\ v_1 \\ v_2 \end{bmatrix} = \begin{bmatrix} \frac{1}{\sqrt{3}} & \frac{1}{\sqrt{3}} & \frac{1}{\sqrt{3}} \\ \frac{1}{\sqrt{6}} & \frac{1}{\sqrt{6}} & -\frac{2}{\sqrt{6}} \\ \frac{1}{\sqrt{6}} & -\frac{2}{\sqrt{6}} & 0 \end{bmatrix} \begin{bmatrix} R \\ G \\ B \end{bmatrix} \quad (5)$$

$$H = \tan^{-1}\left(\frac{v_2}{v_1}\right) \qquad I = \frac{(R+G+B)}{3} \qquad S = \sqrt{v_1^2 + v_2^2}$$

$$\begin{bmatrix} R \\ G \\ B \end{bmatrix} = \begin{bmatrix} \frac{1}{\sqrt{3}} & \frac{1}{\sqrt{6}} & \frac{1}{\sqrt{2}} \\ \frac{1}{\sqrt{3}} & \frac{1}{\sqrt{6}} & -\frac{1}{\sqrt{2}} \\ \frac{1}{\sqrt{3}} & -\frac{2}{\sqrt{6}} & 0 \end{bmatrix} \begin{bmatrix} I \\ v_1 \\ v_2 \end{bmatrix}$$

4.2.2. BROVEY method

Brovey is a numerical method in which images are combined by normalizing the pixel values in multispectral image bands and then multiplied by the value of the corresponding pixels in the panchromatic

image. In numerical methods, addition and multiplication and the ratio between different bands of multispectral image and panchromatic image are used (Aiazzi et al., 2007). The general equation of this method is as follows:

$$BT_i = \frac{MS_i}{\sum_i^n MS_i} PAN \quad (6)$$

In which the BTi_i of the band i from combined image, the MS_i of the band i from the multispectral image, and PAN is a panchromatic image with high spatial resolution.

5.2.2. Wavelet method

In this method, the spatial information in the panchromatic and multispectral image is extracted by direct wavelet conversion, and the spatial information in the panchromatic image is replaced with or added to the spatial information in the multispectral image. Then, reverse wavelet conversion is done on the conversion coefficients of the converted wavelet of multispectral image (Park & Kang, 2004). The basis of this method is resembles the IHS method and includes the following 6 steps:

1) Converting pixel dimensions of multispectral image to panchromatic image 2) Applying IHS conversion to multispectral image and using I, H and S parameters 3) Creating new "P" panchromatic image according to figure I 4) "P" decomposition through wavelet decomposition, also two components of the wavelet image $y_1^{(p)}$ and $y_2^{(p)}$, and an approximate image of P_2 are estimated. Moreover, it is repeated for I. Two components of wavelet image $y_1^{(1)}$ and $y_2^{(1)}$, and an approximate image of I_2 are estimated. 5) Calculation of the difference: $\delta = I^{\%} - I = \sum_K y_k^{(p)} - \sum_k y_k^{(1)}$ where $\sum_k y_k^{(p)} = y_1^{(p)} + y_2^{(p)}$ and $\sum_k y_k^{(I)} = y_1^{(1)} + y_2^{(1)}$

6) Adding spatial information of panchromatic images to multispectral images by reverse IHS conversion (Gungor & Shan, 2004).

194 (7) $$\begin{pmatrix} \hat{R} \\ \hat{G} \\ \hat{B} \end{pmatrix} = \begin{pmatrix} R + (I\hat{} - I) \\ G + (I\hat{} - I) \\ B + (I\hat{} - I) \end{pmatrix} = \begin{pmatrix} R + (\sum y_k^{(p)} - \sum y_k^{(I)}) \\ G + (\sum y_k^{(p)} - \sum y_k^{(I)}) \\ B + (\sum y_k^{(p)} - \sum y_k^{(I)}) \end{pmatrix}$$

195 6.2.2. Principal Component Transformation Method

196 Multispectral data can be visualized in a multidimensional space. The dimensions of this space will be the
197 same as the number of image bands, in which each pixel is considered as a vector. The main goal in principal
198 component transformation is to get new components in which the data variance is higher and the
199 dependence between the components is less than the initial state of the images. The fusion of data at the
200 pixel level, which is also called image fusion, has a great variety of algorithms. For this reason, in various
201 applications, researchers have tried to study and analyze the methods used to combine images, and consider
202 classifying the methods, their advantages and disadvantages (Rockinger, 1996). In this research, PCS
203 method is used as one of the main methods of principal component transformation.

204

205 3.2. Evaluation methods for image fusion quality

206 Approximate evaluation itself is not adequate for image fusion, and different quantitative criteria have been
207 suggested for evaluating combined images (Yang et al., 2012). The aim of spectral quality assessment is to
208 measure the qualitative similarity of the image combined with the original one and to determine the degree
209 of changes and disturbances in the image quality as a result of calculations and combination process.

210 In this research, three evaluation criteria have been used such as correlation criteria, ERGAS and RMSE.
211 In table 3, calculation method and the concept of each of these indices have been mentioned completely.

212

213

214

215 Table3. indices for evaluation of image combination quality

Index	Formula	Comments
CC[10]	$CC(\frac{R}{F}) = \frac{\sum_{J=1}^{N}\sum_{i=1}^{M}(R(i,j)-\mu(R))(F(i,j)-\mu(F))}{\sqrt{\sum_{i=1}^{N}\sum_{i=1}^{N}((R(i,j)-\mu(R))^2(F(i,j)-\mu(F))^2}}$ F and R are basic and combined images, μ (R) and μ (F) are the mean of the two images	The closer this value is to 1, the greater the degree of correlation between the two images. In order for the data to be more homogenized with the mean, this index provides a better estimation to compare the combination result (Choi et al., 2013).
RMSE[11]	$RMSE = \sqrt{\frac{\sum_{i=1}^{M}\sum_{j=1}^{N}(R(i,j)-F(i,j))^2}{M \times N}}$ Pixels N * M Image dimension	The closer this value is to zero, the better combination and the less error is (De Carvalho & Meneses, 2000).
ERGAS[12]	$ERGAS = 100\frac{h}{l}\sqrt{\frac{1}{N}\sum_{i=1}^{N}(RMSE^2/L^2)}$ h: The spatial resolution of the panchromatic band and l: The resolution of the primary image band, N: Number of bands used L: radiation mean	It is sensitive to the displacement mean and change of dynamic rate. If the value is less than 3, it means that the result of the combination is satisfactory and the combined image is of good quality. Because this index is independent of the unit, it somehow involves the spatial resolution of the source images (Alparone et al., 2004).

216

217

218 3.3. Classification methods

219 In this section, in order to summarize the article, classification methods in this study will be explained
220 briefly. Readers are kindly asked to follow available references in each section.

221

222 3.3.1. Maximum Likelihood method

[10] Correlation Coefficient
[11] Root Mean Squared Error
[12] Error Relative Global Dimensional Synthesis

The maximum likelihood method (the most similarity) is one of the most popular and practical methods of supervised information classification (Zurita-Milla et al, 2006). In this method, the likelihood that a pixel might belong to all classes is calculated, and that pixel will belong to the most likely class (Chen et al., 2009).

3.3.2. Fuzzy Artmap method

Fuzzy artmap is a neural network introduced in 1991 by Carpentz et al. It is based on adaptive resonance theory (Mather & Koch, 2011). In this method, the classification is controlled by three parameters: the consciousness parameter (ρ), the learning parameter (β), and the base parameter (α). The value of consciousness parameter (ρ) is between 0 and 1. Values close to 1 indicate strong clustering.

Learning parameter (β) demonstrates the speed of network learning. Finally, the weight vector layer (Wj) is obtained, which depends on the classification of each output and the input data. Furthermore, a weight matrix is also provided with all output clusters. The α parameter shows the number of subclasses that have been created and is usually a number close to zero (Carpenter et al., 1991)

3.3.3. Classification of multilayer perceptron layer

Multilayer perceptron network is usually taught by back propagation (Bp) method. There is no connection between neurons of a layer in the back propagation learning law (Bp). However, the output of each neuron is connected to the input of the next layer neurons.

The teaching and learning process requires a set of educational models with optimal inputs and outputs (Gil-Sánchez et al., 2015). In general, there are two steps to classify a neural network. The first step is the educational process by input data and instructional examples. The second stage is the validation stage, which determines the success of the educational stage and the accuracy of the network (Wijaya, 2005).

4.3.3. Tree classification method

Tree classification by sequentially dividing the data in each internode proceeds to new internodes containing more homogeneous subsets of educational pixels. A newly created internode may create a leaf if the teaching pixels contain only one class or the majority of the pixels with a class. When there is no branch for separation, the final rules of tree classification are formed (Yuan et al., 2005).

5.3.3. Minimum-distance-to-means classification method

In this method, first the mean of all classes, which have been previously separated by the method of determining the educational areas, is determined, and then the Euclidean distance calculates the reflection of each pixel from the mean of all classes. This type of classification is mathematically simple and computationally efficient. However, its theoretical foundations are not as strong as those of maximum likelihood classification (Vogelmann et al., 2001).

Kappa coefficient parameters and overall accuracy were used to estimate the validation of classification maps. The overall accuracy calculates the precision based on the ratio of the correct classified pixels to the sum of the total known pixels, but the Kappa coefficient calculates the accuracy of the classification over a completely random classification (Mather & Tso, 2016). To compare the classification maps, 1,700 points were selected as a regular network at the study area (Figure 3), and in these areas the estimated type of coverage was compared with the combined images. In the separation of pistachio trees from weeds, the original image taken with the UAV was used as a basis, and in the classification of different pistachio cultivars, a map prepared through harvesting was used for validation.

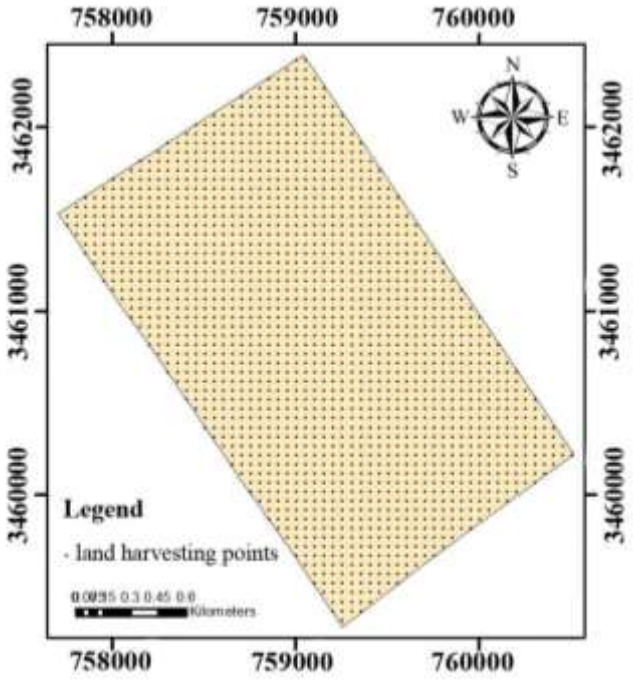

Figure 3. Location of land harvesting points to evaluate accuracy

4. Result and Discussion

4.1. Selection of optimal method to combine UAV and Landsat images

The ultimate goal of image fusion is to get an image that has a higher spatial resolution. The main necessity of all proposed methods in the process of image fusion is to maintain or make the least change in the spectral information of the input images. The purpose of quality assessment is to obtain quantitative and qualitative estimation of the image and also to compare the relative efficiency of different image fusion algorithms. Figure 4 shows the results of using data combination algorithms at the pixel level such as based on high-pass filter, wavelet, Principal Component Transformation, BROVEY, IHS, and Gram Schmidt. After combining Landsat 8 bands with UAV images using the mentioned algorithms, it was observed that these images could be interpreted visually more than the main images. Based on the results, each of these algorithms have had different functions. Mostly these differences are due to keeping details. Meanwhile, the results from PCS algorithm show that there are more blurring parts. Nearly all algorithms functioned well in terms of visual quality (blurring and keeping details and sides), except for the HPF algorithm, which

significantly degrades image quality. Approximate assessment alone is not adequate to combine images, and different quantitative criteria have been suggested to evaluate the combined images. When Landscape and UAV images are combined to create a new image with a spatial resolution of 20 cm, there is no image as a reference for comparison to assess its accuracy, and primary Landsat images are used to assess spectral accuracy. The results of quality assessment present six methods of combining the images applied on the desired bands in table 4. The parameters used to evaluate accuracy indicate the superiority of the wavelet method over other methods. The value of the linear correlation between each band was calculated from the combined and the reference images, and the average value of the correlation was the final criterion for evaluation. The value of correlation in the combined images and the base image using the methods based on high-pass filter, wavelet, Principal Component Transformation, BROVEY, IHS and Gram Schmidt methods were 0.63, 0.91, 0.74, 0.88, 0.8, and 0.79 respectively, which indicates a strong resemblance between the combined images and the base images. In the RMSE component, the wavelet method with a value of 12.22 cm has a better result than other combined methods. This index is better than the correlation coefficient and has a higher sensitivity compared to the correlation coefficient index (McHugh, 2012). Therefore, if the function of the two fusion methods is the same compared to the correlation coefficient, the RMSE index can be used to distinguish the better method. The wavelet and BROVEY methods have a close correlation coefficient, but the RMSE rate is lower in the wavelet method and has led to better quality in spectral accuracy evaluation. ERGAS error evaluation criteria in methods based on high-pass filter, wavelet, Principal Component transformation, BROVEY, IHS, and Gram Schmidt methods are 8.43, 2.05, 7.98, 3.79, 4.17 and 5.52 respectively. In fact, this criterion indicates the amount of spectral deviation in the final image fusion. The lower the ERGAS value, the closer the combined image is to the reference image. The results of this criterion indicate the higher efficiency of the wavelet method over other methods. The results of the evaluation of three criteria showed that the wavelet method increases the spatial resolution accuracy by maintaining the spectral information of the image.

Since spatial resolution is one of the factors which determines the accuracy of classification, the combined image was used by the wavelet method to classify and separate weed cover and pistachio tree cultivars. In fact, it will help to classify different vegetation.

Table 4. Values of evaluation indices between the corresponding bands in the combined images and Landsat image bands

Index	Brovey	IHS	PCS	HPF	gram-schmidt	Wavelet
CC	0.88	0.8	0.74	0.63	0.79	0.91
RMSE (cm)	16.09	20.55	34.9	47.80	28.4	12.22
ERGAS	3.79	4.17	7.98	8.43	5.52	2.05

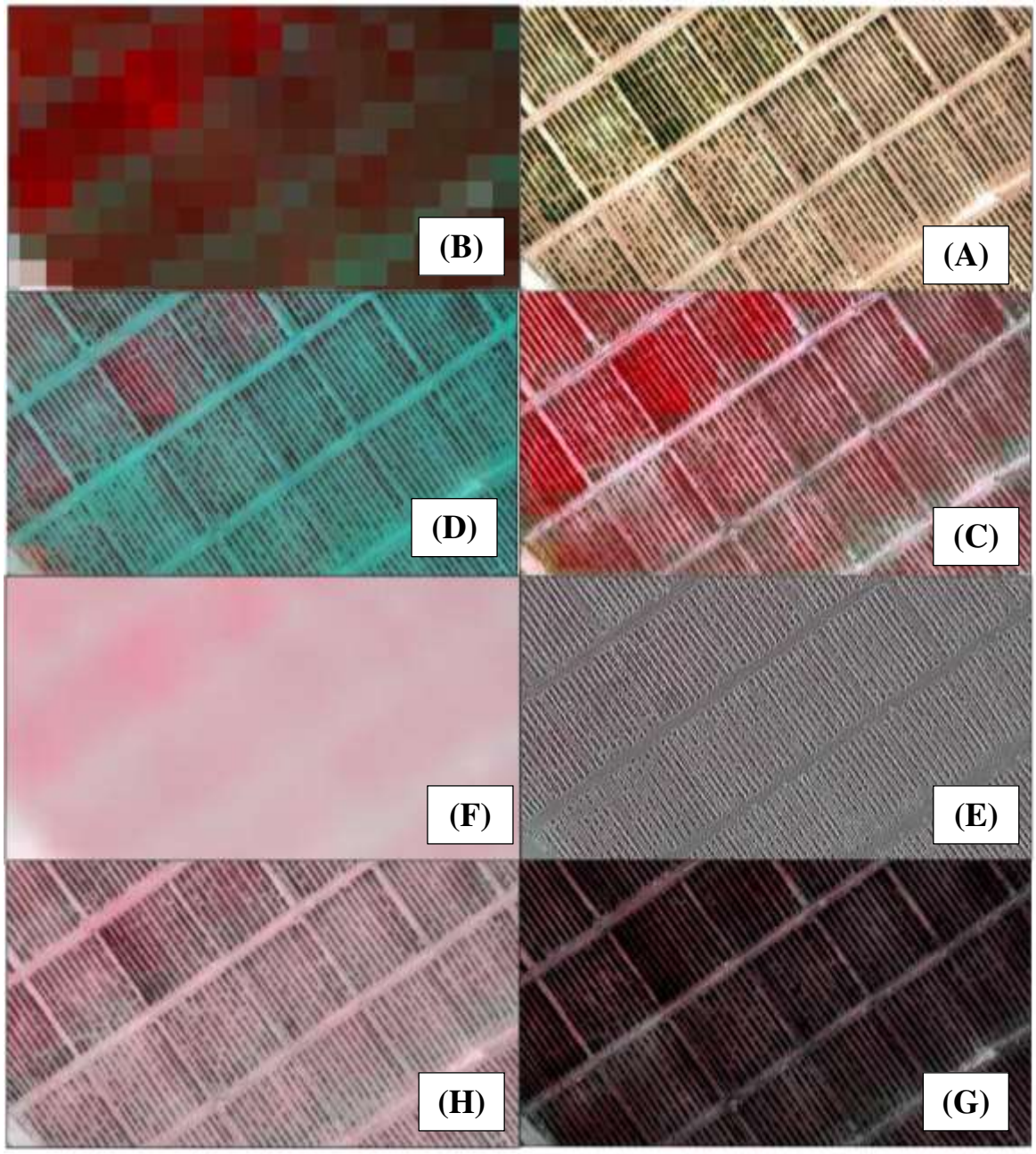

Figure 4. Compare the false color combination of the images A) UAV B) Landsat C) Image obtained from IHS method D) Wavelet E) HPF F) PCS G) Grammy Schmidt H) BROVEY

4.2. Comparison between different methods of classification of pistachio cultivars and weed separation from trees

Researchers have identified the date of satellite imagery and its proximity to the time of growth and emergence of the agricultural crop as essential for identifying areas covered by plants and crops (Pradhan et al,. 2006). In this study, according to the information obtained from the vegetative period of the products and their phenology, the imaging date of the UAV was determined and the closest Landsat 8 image to that time was prepared so that the separation of different products would be possible through having maximum absorption and reflection of the plant in different bands.

Classification of land areas was carried out to categorize different cultivars of pistachios and separate weed and pistachio trees via UAV images, Landsat images and combined images. Moreover, different classification methods including unsupervised classification methods, maximum likelihood, minimum distance, fuzzy artmap, perceptron, and tree classification was evaluated. Six classes including soil, pistachio cultivars of Ahmad Aghaei, Akbari, Kalleh Ghoochi, Fandoghi and combined class of Kalleh Ghoochi and Fandoghi were extracted to classify pistachio cultivars. Also, three soil classes, pistachio tree and weed were chosen to separate weeds from trees. In order to evaluate the accuracy of the classified maps by different methods, classified maps were compared with the map obtained from the field studies. Then, confuse matrix was formed, and the overall accuracy and kappa coefficient were calculated (Tables 5 and 6). It is impossible to identify the weed-covered area and separate it from pistachio trees through Landsat images, and this classification was done only with the combined images and UAV images. The results of the accuracy assessment indicated that the kappa coefficient, overall accuracy and validation using harvesting in the fuzzy artmap classification method by the combined image were 87.0, 84.2 and 87.34 and in the UAV image were 0.76, 81.6 and9 5.12 respectively and it was higher in comparison with other methods and it is correspondent to the results of Farsani et al. (2015) and Williams (1992). They are followed by the maximum likelihood, minimum distance, unsupervised, tree classification, and perceptron methods respectively. The perceptron method could not distinguish pistachio areas from weeds and only recognized weed and soil use. Also, unsupervised classification did not distinguish weeds from pistachio trees. Landsat images alone cannot distinguish weeds from pistachio trees, and the use of combined images

of UAVs and Landsat, with a spatial resolution of 20 cm, can detect weeds and prevent the mixing of soil reflections and vegetation. The results of this study are based on the results of the research done by of An & Shi (2014), Dhruval & Richard (2015), and Gungor, & Shan (2004). And that is about improvement of satellite data interpretation through wavelet fusion and the ability to combine UAV images with other sensors to accurately manage agriculture with the results of Morgan et al. (2017).

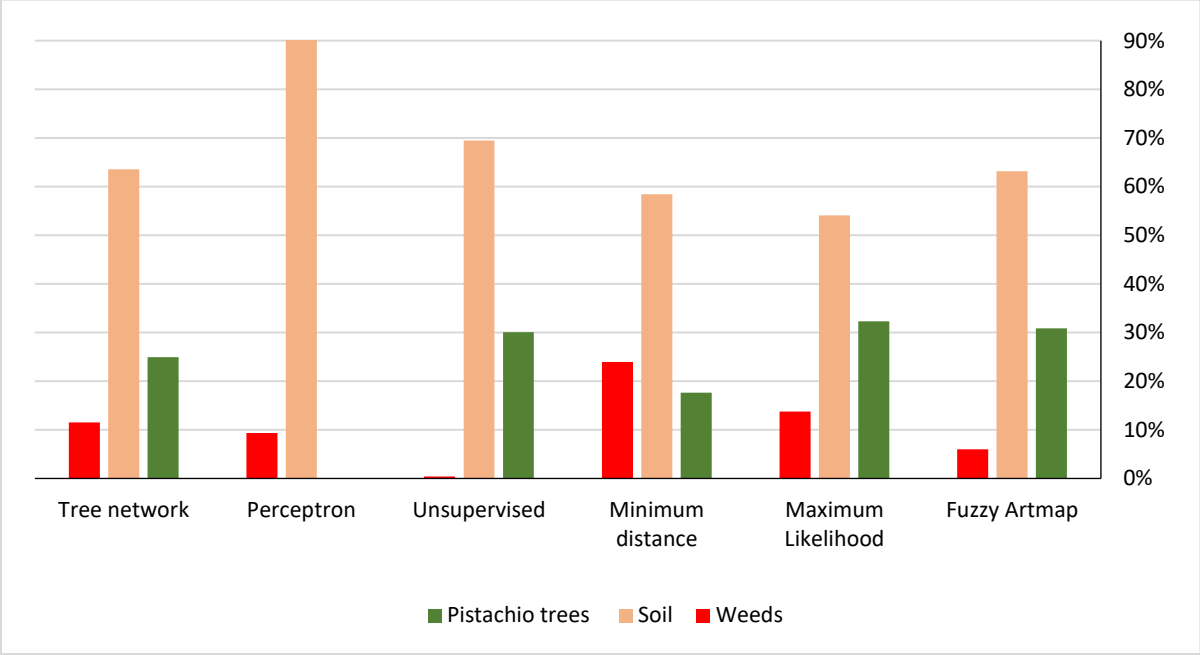

Figure 5. Comparison of weed, soil and tree area in different classification methods (unsupervised method, maximum likelihood, minimum distance, fuzzy artmap) using combined UAV and Landsat images

A section from the area under study with six classification methods is shown in Figure 6. In all classification methods, soil contains the highest area, then pistachio and weed are in the following. In the fuzzy artmap method, which is known as the optimal method to separate weeds from pistachio trees, 6% of the area is covered with weeds, 22% contains pistachio trees and 70% is soil. Figure 7 shows a map of separation of pistachio trees from weeds by fuzzy artmap method.

Table 5. Comparison between the accuracy of different classification methods for weed separation from trees through combined image and UAV images.

Classification method	combined UAV and Landsat images			UAV images		
	Kappa coefficient	Overall accuracy (%)	Validation through harvesting (%)	Kappa coefficient	Overall accuracy (%)	Validation through harvesting (%)
Minimum distance	0.76	83.2	80.05	0.65	76.9	76.91
Fuzzy artmap	0.87	89	94.48	0.76	81.6	95.12
Perceptron	0.21	23.09	67.26	0.20	21.57	63.76
Tree network	0.70	79.56	75.3	0.62	73.91	71.49
Maximum likelihood	0.85	84.2	87.34	0.77	81	74.23
Unsupervised	0.73	74.3	90.23	0.65	69.8	88.68

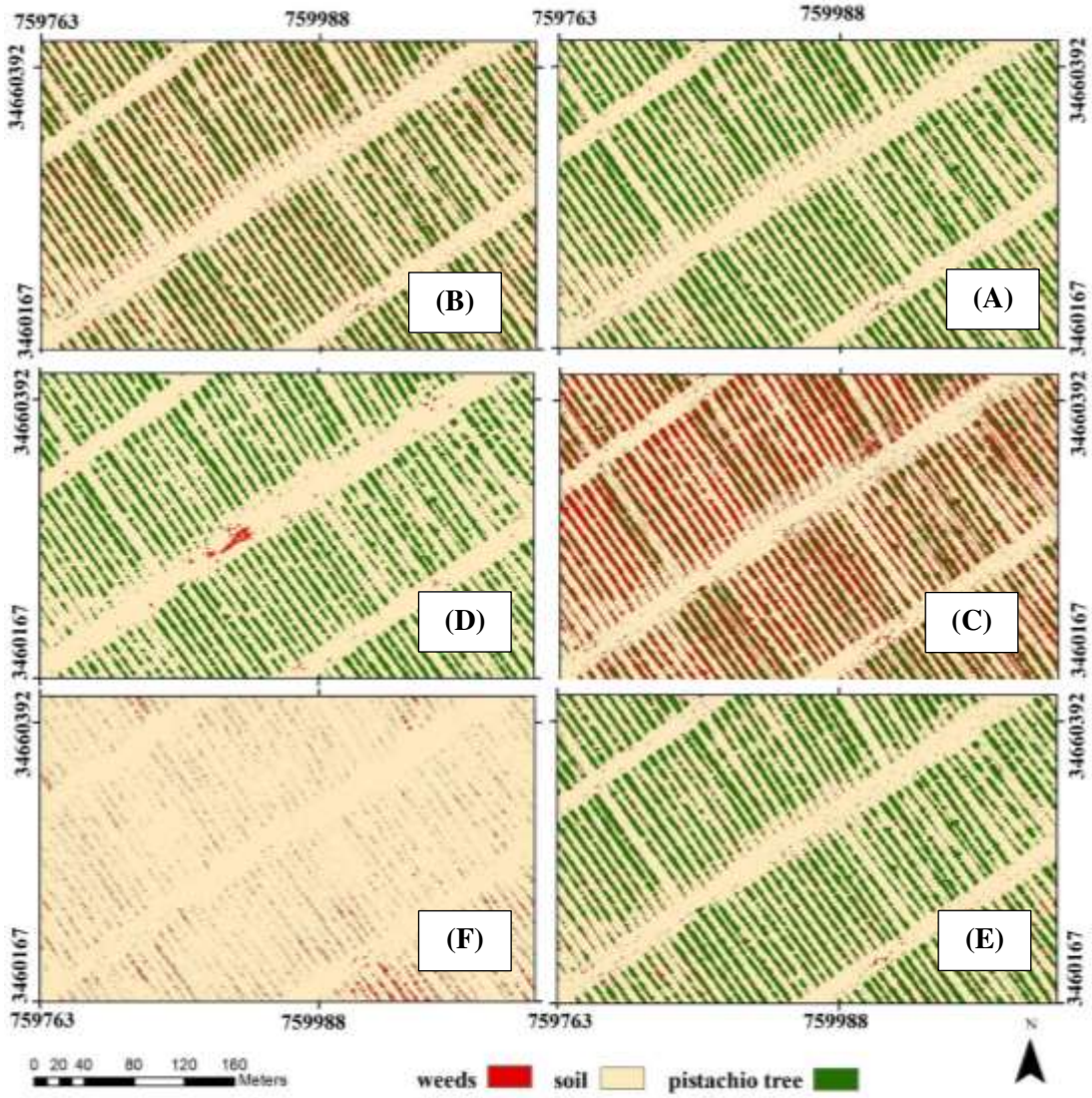

Figure 6. Comparison between different classification methods to separate weeds from pistachio trees using combined UAV and Landsat images A) maximum likelihood B) fuzzy artmap C) minimum distance D) tree network E) unsupervised F) perceptron

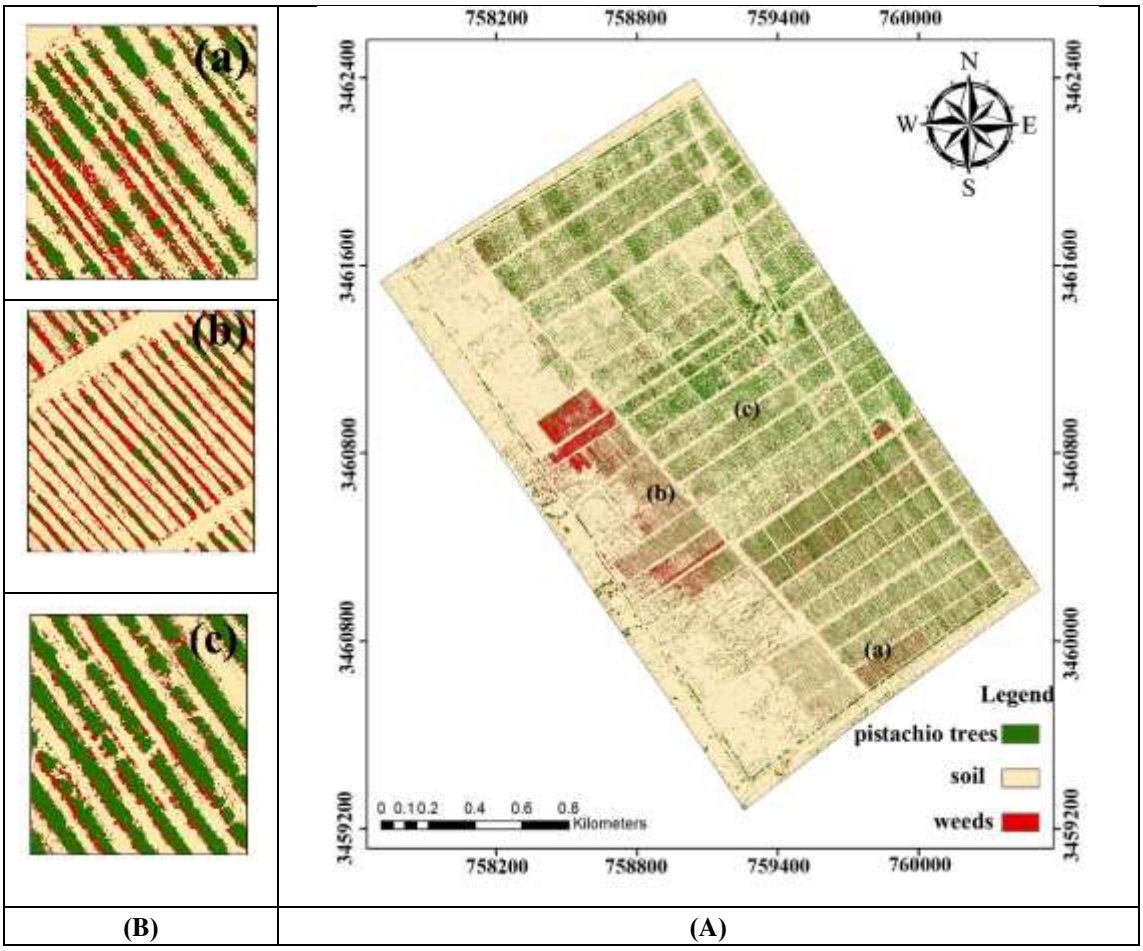

Figure 7. A) Map of separating the use of pistachio trees from weeds by fuzzy artmap method using combined UAV and Landsat images, B) Close perspective of 3 points in the map of separation of pistachio trees from weeds

Then, the classification of different pistachio cultivars was done by Landsat and combined images. The results of the accuracy assessment showed that the kappa coefficient, overall accuracy and validation through harvesting in the fuzzy artmap classification method based on Landsat images were 0.79, 0.82 and 73.05 respectively. Also, in comparison with other methods of accuracy, it was more accurate. In the classification using combined images and UAV images, the highest accuracy was related to fuzzy artmap method with kappa coefficient of 0.87 and 0.83. The results of the validation through harvesting showed that out of 1700 selected points, pistachio cultivar points were correctly identified in 90.47%. Estimation of the area of different pistachio cultivars showed that 70% of the area was soil and 8.2, 8.7, 9.5, 1.8 and 1.1%, contained Akbari, Fandoghi, Kalleh Ghooch & Fandoghi, combined class of Ahmad Aghaei and

Kalleh Ghoochi cultivars respectively. The present study showed the results of the study of Perma et al. (2009) [71] who stated that in preparing forest maps using LISS III and ETM + satellite data, due to the openness of the canopy and mixing of soil reflection and vegetation, it prevents the achievement of more desirable results. It has been corrected and shown that by combining Landsat and UAV images and increasing spatial resolution, it is possible to prevent the mixing of soil reflection and vegetation in classifying vegetation types. The classified maps, which are used to separate pistachio cultivars and usually prepared by Landsat, combined and base image through ground sampling, are shown in Figure 8.

Table 6. Comparison between the accuracy of pistachio cultivar classification methods using Landsat image and combined image

Classification method	Landsat image			UAV images			combined image		
	Kappa coefficient	Overall accuracy (%)	Validation through harvesting (%)	Kappa coefficient	Overall accuracy (%)	Validation through harvesting (%)	Kappa coefficient	Overall accuracy (%)	Validation through harvesting (%)
Minimum distance	0.56	75	50.19	0.55	59	60.82	0.58	61	62.13
Fuzzy artmap	0.79	82	73.05	0.83	86	87.03	0.87	88	90.47
Perceptron	0.46	48	37.81	0.21	22	36.43	0.23	26	38.40
Tree classification	0.67	70	58.2	0.71	74	67.09	0.74	77	72.69
Maximum likelihood	0.74	75	69.51	0.78	80	76.38	0.80	83	83.23
Unsupervised	0.34	35	21.68	0.49	57	37.41	0.60	0.64	53.64

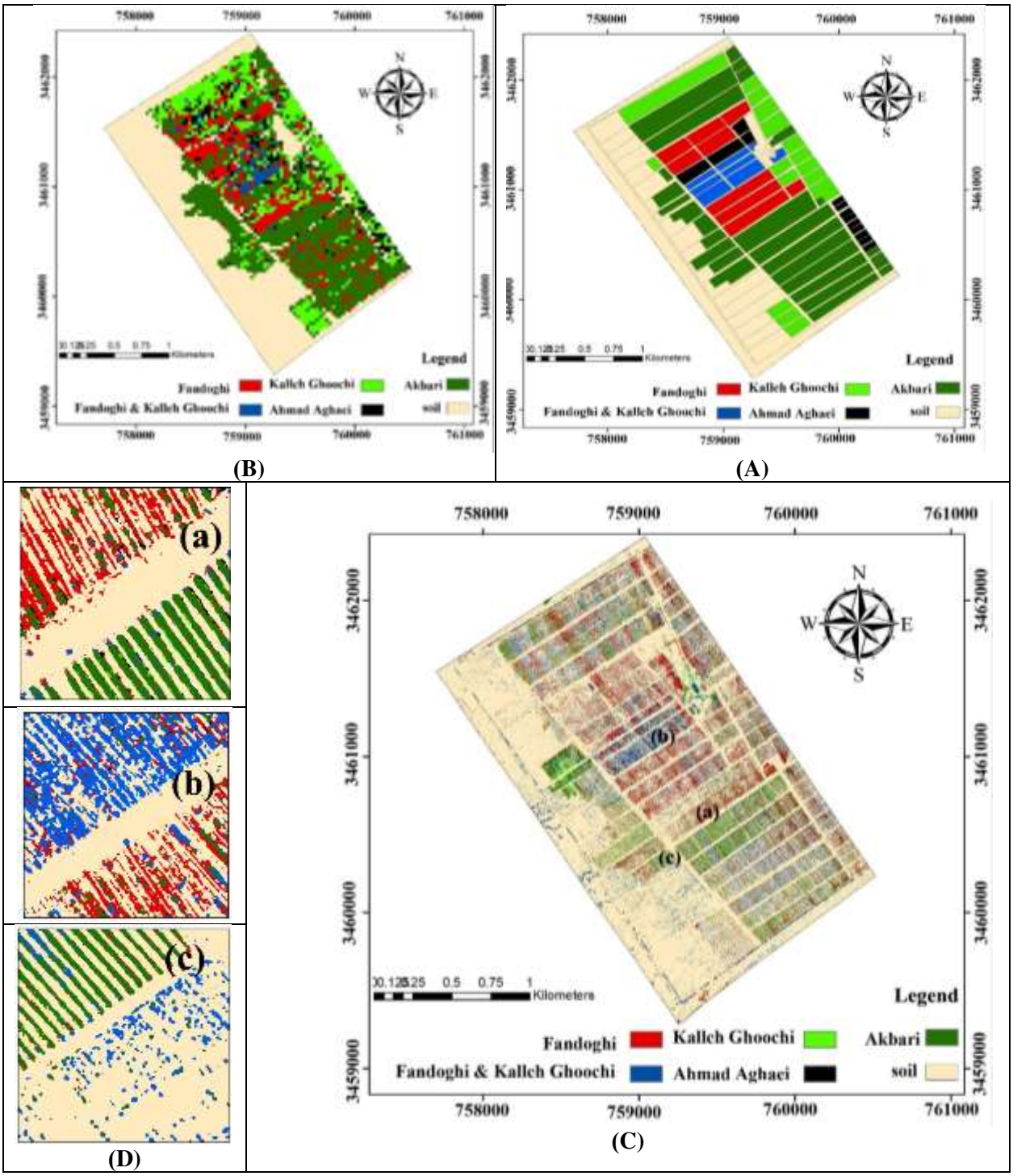

Figure 8.A) Classification of different pistachio cultivars based on the initial cultivation pattern B) Classification of pistachio cultivars using Landsat image C) Classification of different pistachio cultivars using a combined image D) Close view of three points in the map of pistachio cultivars with Use a combined image of UAVs and Landsat

5. Conclusion

Methods of satellite image fusion improve the quality of the spatial resolution of the image and increase the details of the combined image. Different methods have been suggested to combine images. If the goal of image fusion is to study agricultural uses, natural resources, and to separate plant species, in addition to increasing the spatial resolution of the image, spectral characteristics must also be kept. Therefore, in order to combine images, a method must be used that has acceptable accuracy and can, in addition to improving the location, maintain the spectral content of multispectral images well. Using the appropriate method through image quality evaluation indices depends on the researcher's goal of combining images. Since the accuracy of classification depends on the spatial information in the image, by comparing the results of combining images, it can be observed that by keeping the spectral information of the image, the spatial accuracy is increased to 20 cm.

The results of comparison between different classification methods to determine different pistachio cultivars and separate weed from trees indicated that the fuzzy artmap method has the highest accuracy following the maximum likelihood method. This study demonstrated that the product resulted by combining UAV and Landsat images gives the chance to separate weeds that cannot be identified with Landsat images, and also increases the accuracy of classification of pistachio tree cultivars. Moreover, it has a high accuracy of land area and cultivation pattern. The present investigation corrected the map of different forest types, which has prevented the achievement of more desirable results because of the openness of the canopy, mixing of soil, and vegetation reflections. In addition, it showed that by combining Landsat and UAV images and increasing spatial resolution, it would be possible to stop the mixing of soil reflection and vegetation. The study of the area under cultivation of different cultivars through satellite data and preparing land maps and determining the area covered by weeds can be effective in optimal management of these land areas and it is a great way to increase efficiency in the area as well.

Reference

[1] Wardlow, B. D., Egbert, S. L., & Kastens, J. H. (2007). Analysis of time-series MODIS 250 m vegetation index data for crop classification in the US Central Great Plains. *Remote sensing of environment*, *108*(3), 290-310.

[2] Hamidy, N., Alipur, H., Nasab, S. N. H., Yazdani, A., & Shojaei, S. (2016). Spatial evaluation of appropriate areas to collect runoff using Analytic Hierarchy Process (AHP) and Geographical Information System (GIS)(case study: the catchment "Kasef" in Bardaskan. *Modeling Earth Systems and Environment*, *2*(4), 1-11.

[3] Tatsumi, K., Yamashiki, Y., Torres, M. A. C., & Taipe, C. L. R. (2015). Crop classification of upland fields using Random forest of time-series Landsat 7 ETM+ data. *Computers and Electronics in Agriculture*, *115*, 171-179.

[4] Emelyanova, I. V., McVicar, T. R., Van Niel, T. G., Li, L. T., & Van Dijk, A. I. (2013). Assessing the accuracy of blending Landsat–MODIS surface reflectances in two landscapes with contrasting spatial and temporal dynamics: A framework for algorithm selection. *Remote Sensing of Environment*, *133*, 193-209.

[5] Chianucci, F., Disperati, L., Guzzi, D., Bianchini, D., Nardino, V., Lastri, C., ... & Corona, P. (2016). Estimation of canopy attributes in beech forests using true colour digital images from a small fixed-wing UAV. *International journal of applied earth observation and geoinformation*, *47*, 60-68.

[6] Zhou, Z., Yang, Y., & Chen, B. (2018). Estimating Spartina alterniflora fractional vegetation cover and aboveground biomass in a coastal wetland using SPOT6 satellite and UAV data. *Aquatic Botany*, *144*, 38-45.

[7] Walker, J. J., De Beurs, K. M., & Wynne, R. H. (2014). Dryland vegetation phenology across an elevation gradient in Arizona, USA, investigated with fused MODIS and Landsat data. *Remote Sensing of Environment*, *144*, 85-97.

[8] Laben, C. A., & Brower, B. V. (2000). *U.S. Patent No. 6,011,875*. Washington, DC: U.S. Patent and Trademark Office.

[9] Shettigara, V. K. (1992). A generalized component substitution technique for spatial enhancement of multispectral images using a higher resolution data set. *Photogrammetric Engineering and remote sensing*, *58*(5), 561-567.

439 [10] Pohl, C., & Van Genderen, J. L. (1998). Multisensor image fusion in remote sensing: concepts, methods and
440 applications" International journal of remote sensing–Vol. 19.
441 [11] Wilson, T. A., Rogers, S. K., & Kabrisky, M. (1997). Perceptual-based image fusion for hyperspectral data. *IEEE*
442 *Transactions on Geoscience and Remote Sensing*, *35*(4), 1007-1017.
443 [12] Barbedo, J. G. A. (2019). A review on the use of unmanned aerial vehicles and imaging sensors for monitoring
444 and assessing plant stresses. *Drones*, *3*(2), 40.
445 [13] Yilmaz, C. S., Yilmaz, V., Gungor, O., & Shan, J. (2019). Metaheuristic pansharpening based on symbiotic
446 organisms search optimization. *ISPRS Journal of Photogrammetry and Remote Sensing*, *158*, 167-187.
447 [14] Murugan, D., Garg, A., Ahmed, T., & Singh, D. (2016, December). Fusion of drone and satellite data for
448 precision agriculture monitoring. In *2016 11th International Conference on Industrial and Information Systems*
449 *(ICIIS)* (pp. 910-914). IEEE.
450 [15] Murugan, D., Garg, A., & Singh, D. (2017). Development of an adaptive approach for precision agriculture
451 monitoring with drone and satellite data. *IEEE Journal of Selected Topics in Applied Earth Observations and*
452 *Remote Sensing*, *10*(12), 5322-5328.
453 [16] Jenerowicz, A., Siok, K., Woroszkiewicz, M., & Orych, A. (2017, November). The fusion of satellite and UAV
454 data: simulation of high spatial resolution band. In *Remote Sensing for Agriculture, Ecosystems, and Hydrology*
455 *XIX* (Vol. 10421, p. 104211Z). International Society for Optics and Photonics.
456 [17] Agarwal, A., Singh, A. K., Kumar, S., & Singh, D. (2018, December). Critical analysis of classification
457 techniques for precision agriculture monitoring using satellite and drone. In *2018 IEEE 13th International*
458 *Conference on Industrial and Information Systems (ICIIS)* (pp. 83-88). IEEE.
459 [18] Zhao, L., Shi, Y., Liu, B., Hovis, C., Duan, Y., & Shi, Z. (2019). Finer Classification of Crops by Fusing UAV
460 Images and Sentinel-2A Data. *Remote Sensing*, *11*(24), 3012.
461 [19] Fareed, N., & Rehman, K. (2020). Integration of Remote Sensing and GIS to Extract Plantation Rows from A
462 Drone-Based Image Point Cloud Digital Surface Model. ISPRS International Journal of Geo-Information, 9(3),
463 151.
464 [20] Goldhamer, D.A. 2005. Irrigation Management chapter of University of California Pistachio Production Manual
465 (2005). Edited by L. Ferguson. pgs. 103-116.

[21] Wald, L. (1999). Some terms of reference in data fusion. *IEEE Transactions on geoscience and remote sensing*, *37*(3), 1190-1193.

[22] Maurer, T. (2013). How to pan-sharpen images using the Gram-Schmidt pan-sharpen method-a recipe. *International archives of the photogrammetry, remote sensing and spatial information sciences*, *1*, W1.

[23] Aiazzi, B., Baronti, S., & Selva, M. (2007). Improving component substitution pansharpening through multivariate regression of MS $+ $ Pan data. *IEEE Transactions on Geoscience and Remote Sensing*, *45*(10), 3230-3239.

[24] Pohl, C., & van Genderen, J. (2014). Remote sensing image fusion: an update in the context of Digital Earth. *International Journal of Digital Earth*, *7*(2), 158-172.

[25] Carper, W., Lillesand, T., & Kiefer, R. (1990). The use of intensity-hue-saturation transformations for merging SPOT panchromatic and multispectral image data. *Photogrammetric Engineering and remote sensing*, *56*(4), 459-467.

[26] Zhang, Y. (2008). Methods for image fusion quality assessment-a review, comparison and analysis. *The International Archives of the Photogrammetry, Remote Sensing and Spatial Information Sciences*, *37*(PART B7), 1101-1109.

[27] Park, J. H., & Kang, M. G. (2004). Spatially adaptive multi-resolution multispectral image fusion. *International Journal of Remote Sensing*, *25*(23), 5491-5508.

[28] Gungor, O., & Shan, J. (2004, July). Evaluation of satellite image fusion using wavelet transform. In *proceedings of 20th Congress ISPRS "Geo-Imagery Bridging Continents* (pp. 12-13).

[29] Rockinger, O. (1996, July). Pixel-level fusion of image sequences using wavelet frames. In *Proceedings of the 16th Leeds Applied Shape Research Workshop* (pp. 149-154). Leeds University Press.

[30] Yang, S., Wang, M., & Jiao, L. (2012). Fusion of multispectral and panchromatic images based on support value transform and adaptive principal component analysis. *Information Fusion*, *13*(3), 177-184.

[31] Choi, Y., Sharifahmadian, E., & Latifi, S. (2013). Performance analysis of contourlet-based hyperspectral image fusion methods. *International Journal on Information Theory*, *2*(1), 1-14.

[32] De Carvalho, O. A., & Meneses, P. R. (2000, February). Spectral correlation mapper (SCM): an improvement on the spectral angle mapper (SAM). In *Summaries of the 9th JPL Airborne Earth Science Workshop, JPL Publication 00-18* (Vol. 9). JPL Publication Pasadena, CA.

494 [33] Alparone, L., Baronti, S., Garzelli, A., & Nencini, F. (2004). A global quality measurement of pan-sharpened
495 multispectral imagery. *IEEE Geoscience and Remote Sensing Letters*, *1*(4), 313-317.
496 [34] Zurita-Milla, R., Clevers, J. G. P. W., & Schaepman, M. E. (2006, September). Landsat TM and MERIS FR
497 image fusion for land cover mapping over the Netherlands. In *Proceedings of the 2nd Workshop of the EARSeL*
498 *SIG on Land Use and Land Cover* (pp. 34-40).
499 [35] Chen, M., Su, W., Li, L., Zhang, C., Yue, A., & Li, H. (2009). Comparison of pixel-based and object-oriented
500 knowledge-based classification methods using SPOT5 imagery. *WSEAS Transactions on Information Science*
501 *and Applications*, *3*(6), 477-489.
502 [36] Mather, P. M., & Koch, M. (2011). *Computer processing of remotely-sensed images: an introduction*. John
503 Wiley & Sons.
504 [37] Carpenter, G. A., Grossberg, S., & Reynolds, J. H. (1991). ARTMAP: Supervised real-time learning and
505 classification of nonstationary data by a self-organizing neural network. *Neural networks*, *4*(5), 565-588.
506 [38] Gil-Sánchez, L., Garrigues, J., Garcia-Breijo, E., Grau, R., Aliño, M., Baigts, D., & Barat, J. M. (2015). Artificial
507 neural networks (Fuzzy ARTMAP) analysis of the data obtained with an electronic tongue applied to a ham-
508 curing process with different salt formulations. *Applied Soft Computing*, *30*, 421-429.
509 [39] Wijaya, A. (2005). Application of multi-stage classification to detect illegal logging with the use of multi-source
510 data. *International Institute for Geo-Information Sience and Earth Observation, Enschede, The Netherlands*.
511 [40] Yuan, F., Sawaya, K. E., Loeffelholz, B. C., & Bauer, M. E. (2005). Land cover classification and change analysis
512 of the Twin Cities (Minnesota) Metropolitan Area by multitemporal Landsat remote sensing. *Remote sensing of*
513 *Environment*, *98*(2-3), 317-328.
514 [41] Vogelmann, J. E., Howard, S. M., Yang, L., Larson, C. R., Wylie, B. K., & Van Driel, N. (2001). Completion of
515 the 1990s National Land Cover Data Set for the conterminous United States from Landsat Thematic Mapper data
516 and ancillary data sources. *Photogrammetric Engineering and Remote Sensing*, *67*(6).
517 [42] Mather, P., & Tso, B. (2016). *Classification methods for remotely sensed data*. CRC press.
518 [43] McHugh, M. L. (2012). Interrater reliability: the kappa statistic. *Biochemia medica: Biochemia medica*, *22*(3),
519 276-282.

[44] Pradhan, P. S., King, R. L., Younan, N. H., & Holcomb, D. W. (2006). Estimation of the number of decomposition levels for a wavelet-based multiresolution multisensor image fusion. *IEEE Transactions on Geoscience and Remote Sensing*, *44*(12), 3674-3686.

[45] An, Z. Shi Z. (2014). An improved-SFIM fusion method based on the calibration process. Optik- International Journal for Light and Electron Optics, 125(14): 3764-3769.

[46] Dhruval L. Richard S. (2015). Advance SFIM technique for image fusion in remote sensing domain. International Journal of Innovative Research in Technology, 2(1): 148-161.

[47] Farsani, F. A., Ghazavi, R., & Farzaneh, M. R. (2015). Investigation of land use classification algorithms using images fusion techniques (Case study: Beheshtabad Sub-basin). Journal of RS and GIS for Natural Resources, 6(1), 91-106, 2015.

[48] Williams, J. A. (1992). Vegetation classification using Landsat TM and SPOT-HRV imagery in mountainous terrain, Kananaskis Country, southwestern Alberta. University of Calgary, p. 126-13,1992.

Figures

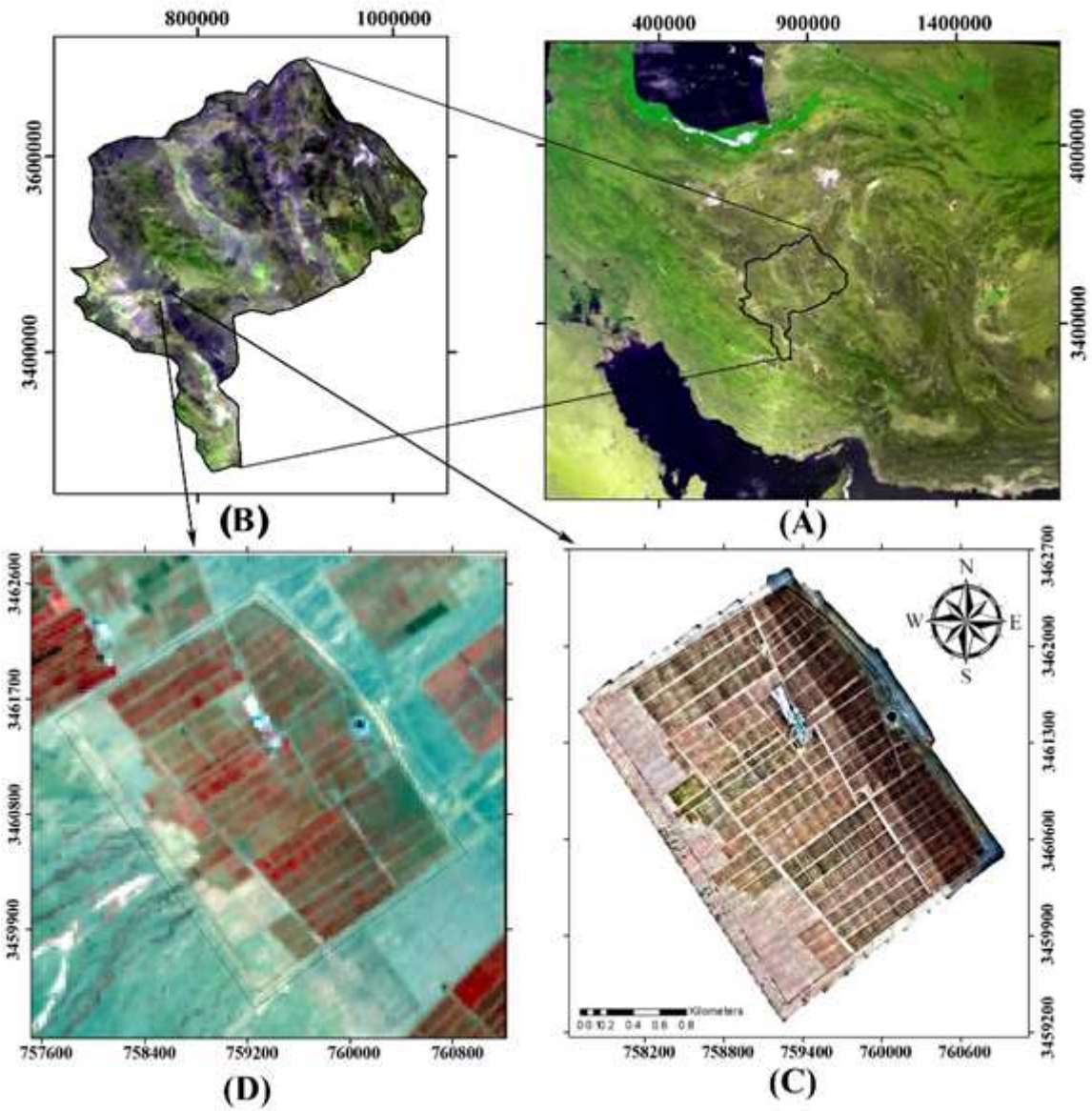

Figure 1

The study area A) Iran B) Yazd province C) Landsat image D) UAV image (08/18/2019) Note: The designations employed and the presentation of the material on this map do not imply the expression of any opinion whatsoever on the part of Research Square concerning the legal status of any country, territory, city or area or of its authorities, or concerning the delimitation of its frontiers or boundaries. This map has been provided by the authors.

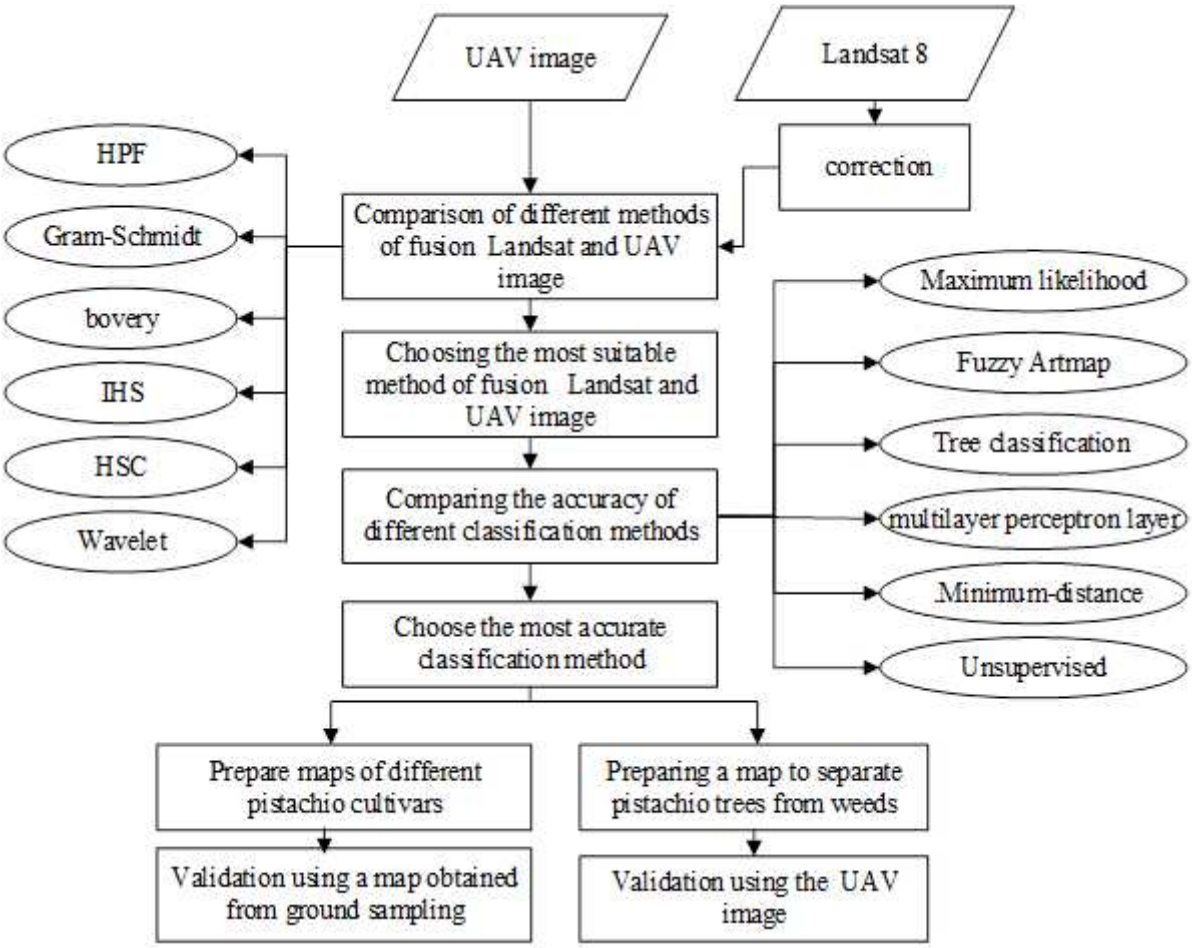

Figure 2

General perspective of the research steps

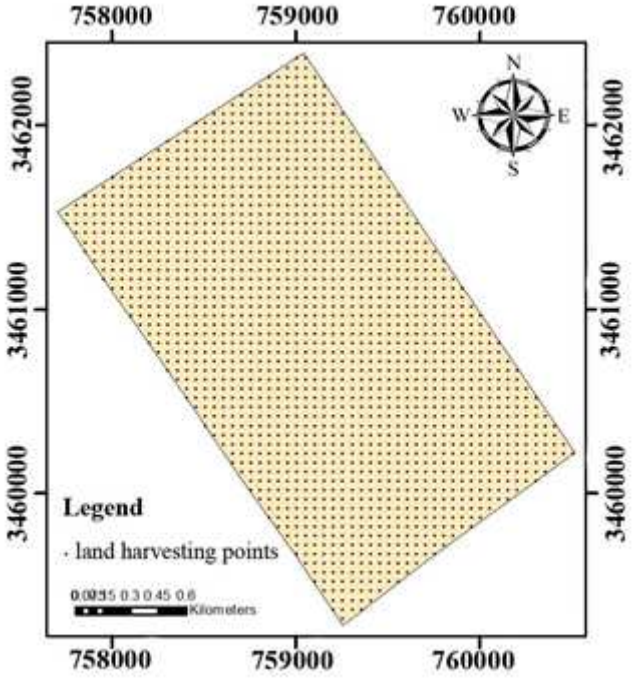

Figure 3

Location of land harvesting points to evaluate accuracy Note: The designations employed and the presentation of the material on this map do not imply the expression of any opinion whatsoever on the part of Research Square concerning the legal status of any country, territory, city or area or of its authorities, or concerning the delimitation of its frontiers or boundaries. This map has been provided by the authors.

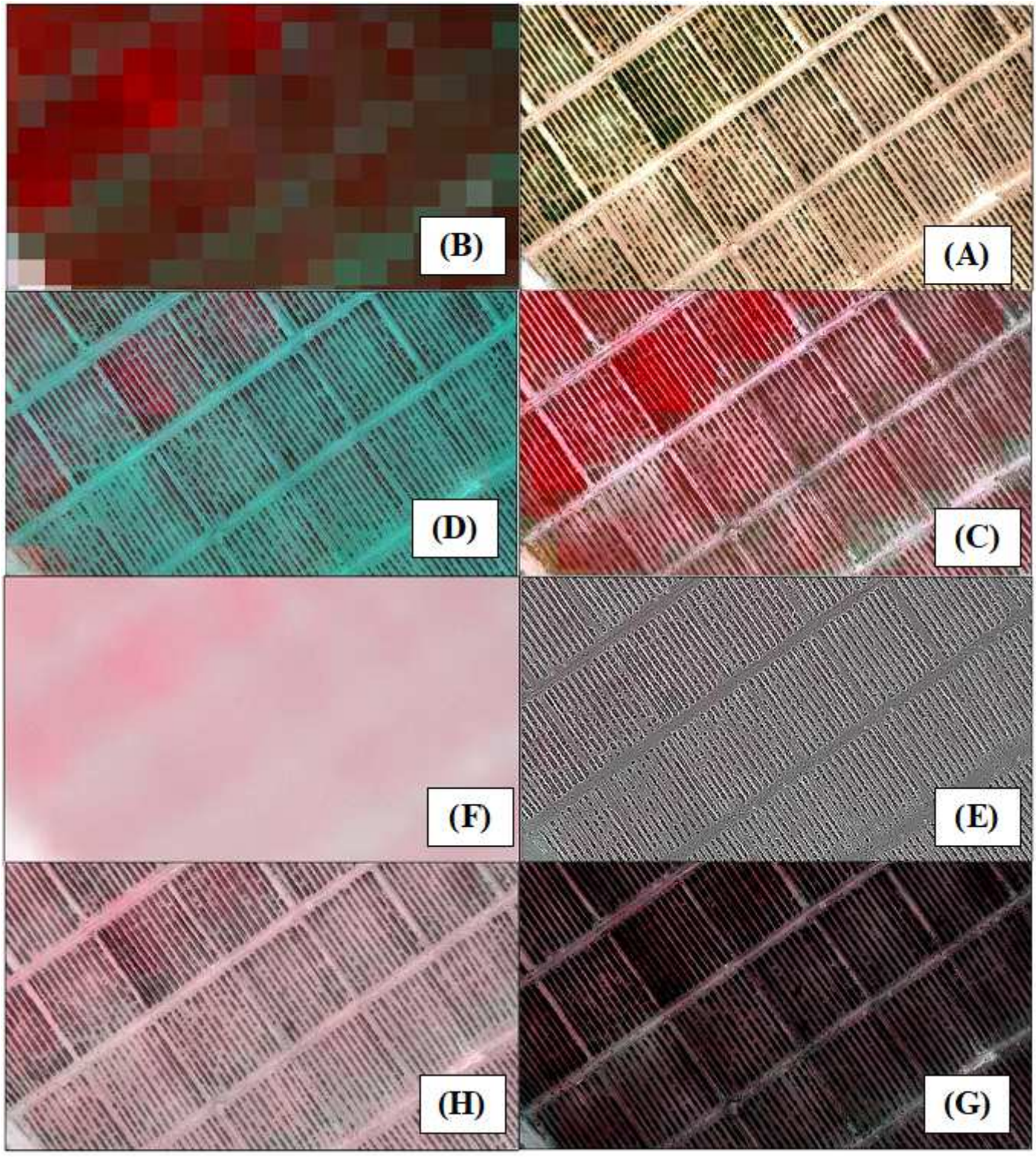

Figure 4

Compare the false color combination of the images A) UAV B) Landsat C) Image obtained from IHS method D) Wavelet E) HPF F) PCS G) Grammy Schmidt H) BROVEY

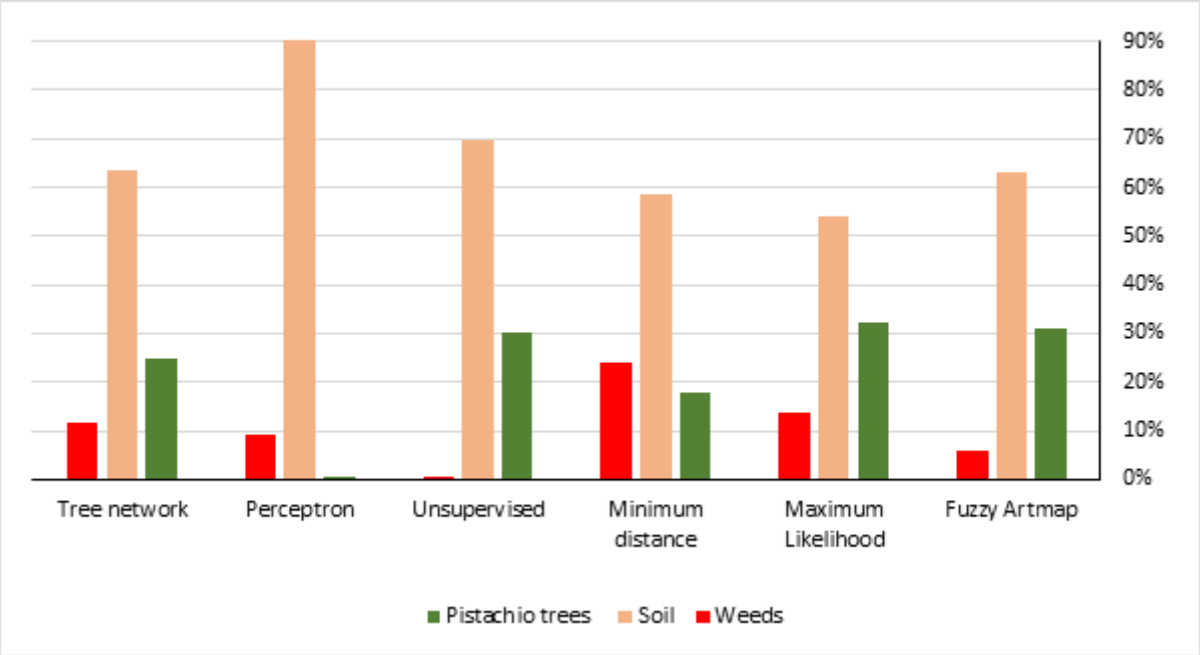

Figure 5

Comparison of weed, soil and tree area in different classification methods (unsupervised method, maximum likelihood, minimum distance, fuzzy artmap) using combined UAV and Landsat images

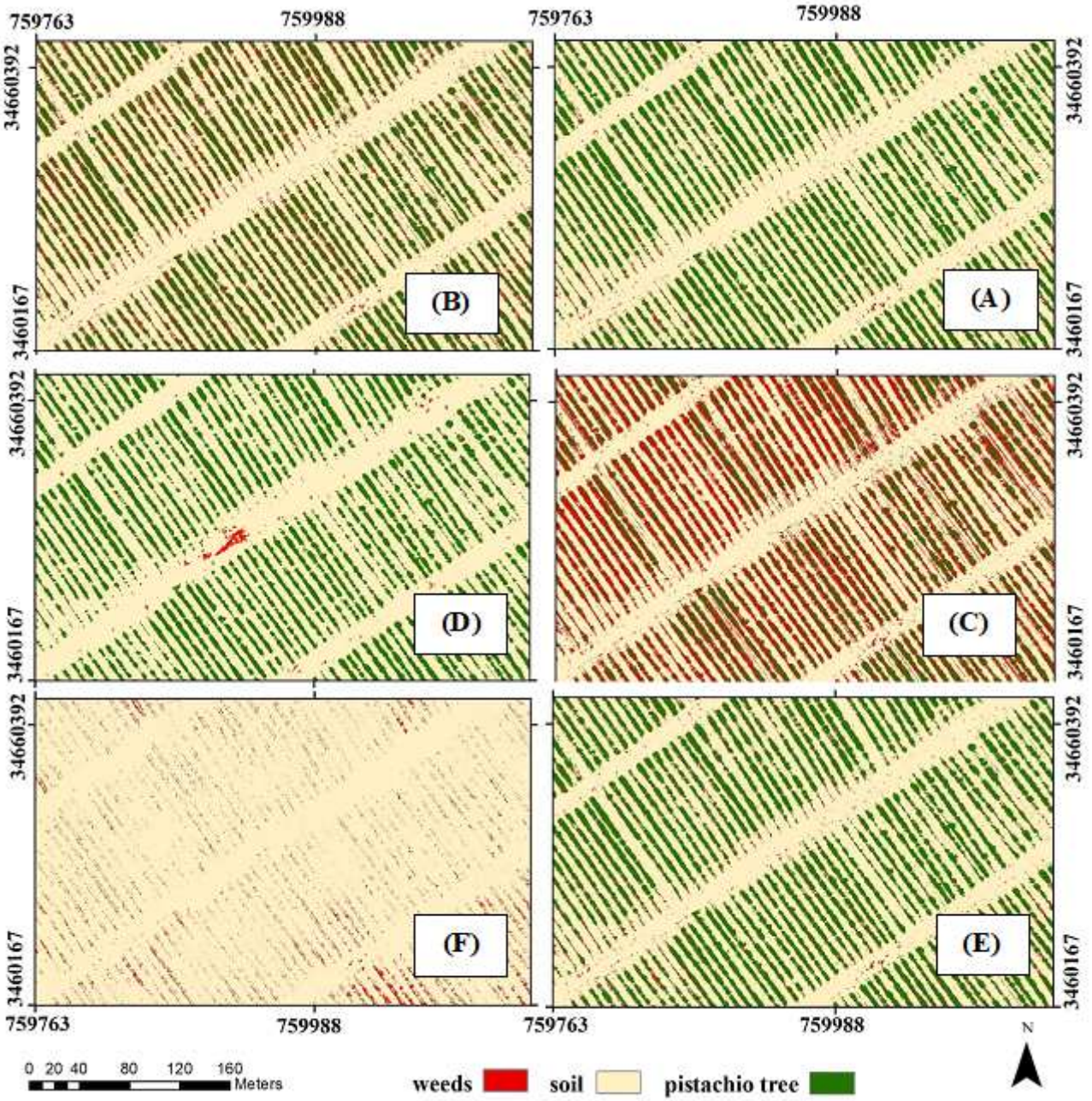

Figure 6

Comparison between different classification methods to separate weeds from pistachio trees using combined UAV and Landsat images A) maximum likelihood B) fuzzy artmap C) minimum distance D) tree network E) unsupervised F) perceptron Note: The designations employed and the presentation of the material on this map do not imply the expression of any opinion whatsoever on the part of Research Square concerning the legal status of any country, territory, city or area or of its authorities, or concerning the delimitation of its frontiers or boundaries. This map has been provided by the authors.

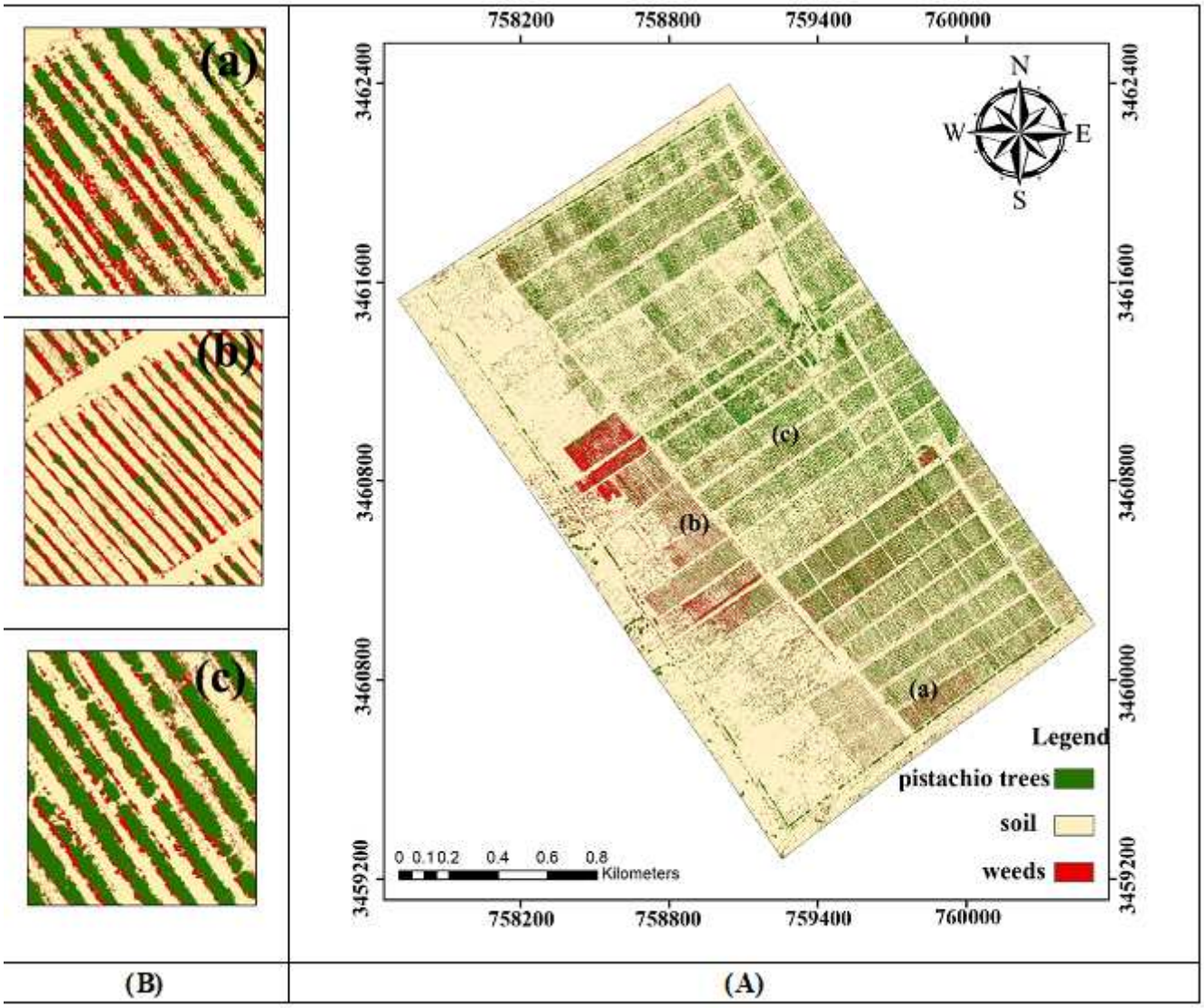

Figure 7

A) Map of separating the use of pistachio trees from weeds by fuzzy artmap method using combined UAV and Landsat images, B) Close perspective of 3 points in the map of separation of pistachio trees from weeds Note: The designations employed and the presentation of the material on this map do not imply the expression of any opinion whatsoever on the part of Research Square concerning the legal status of any country, territory, city or area or of its authorities, or concerning the delimitation of its frontiers or boundaries. This map has been provided by the authors.

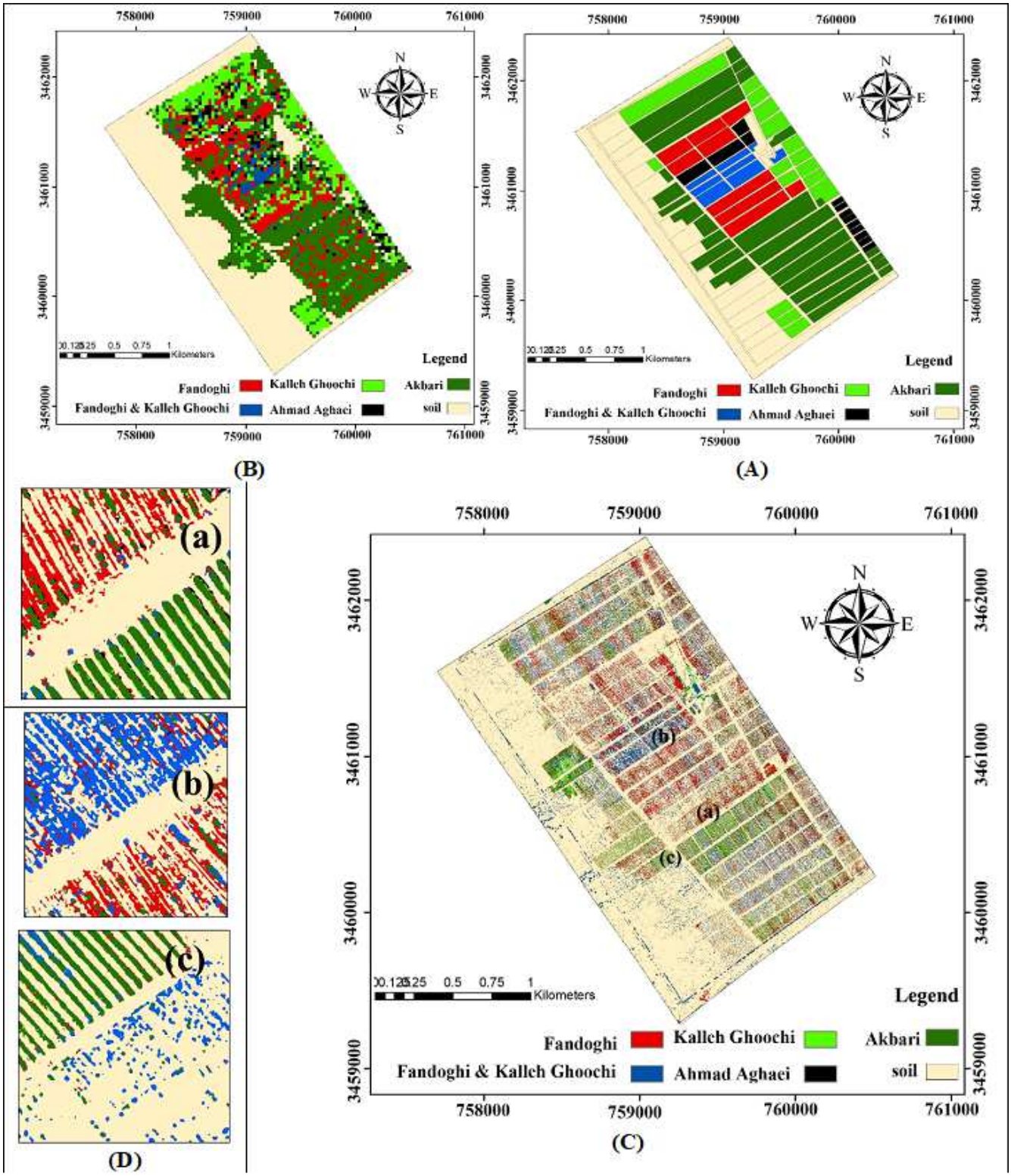

Figure 8

A) Classification of different pistachio cultivars based on the initial cultivation pattern B) Classification of pistachio cultivars using Landsat image C) Classification of different pistachio cultivars using a combined image D) Close view of three points in the map of pistachio cultivars with Use a combined image of UAVs and Landsat Note: The designations employed and the presentation of the material on this map do not imply the expression of any opinion whatsoever on the part of Research Square

concerning the legal status of any country, territory, city or area or of its authorities, or concerning the delimitation of its frontiers or boundaries. This map has been provided by the authors.